Magnetoacoustics of ferrites and magnetoacoustic resonance

O. Yu. Belyaeva, S. N. Karpachev and L. K. Zarembo

M. V. Lomonosov Moscow State University

(Submitted 19 June, 1991; resubmitted after revision 18 September, 1991)
Usp. Fiz. Nauk **162**, 107–138 (February 1992)

A review is given of theoretical and experimental papers on the interaction of acoustic waves with spin waves in ferridielectrics. The region of the resonance interaction—the magnetoacoustic resonance (MAR), in which the interaction is synchronous and is most effective, is discussed in greatest detail. Considerable attention is devoted to nonlinear magnetoacoustic resonance—i.e. to detection of MAR not by absorption, but by generation of higher harmonics of the acoustic wave. The review also discusses the possibilities of using MAR for studying the magnetic and defect structures of crystalline ferridielectrics. The review encompasses practically all the basic papers in this field. The experimental results are systematized, and their correspondence with theory is analyzed.

INTRODUCTION

Acoustic wave propagation in magnetically ordered materials and its dependence on various magnetic fields has been studied by magnetoacoustics for several decades. The magnetic ordering of high-quality magnetic single crystals can be rather high. It provides a possibility of efficient observation of interesting magnetoelastic coupling phenomena. The latter can be divided into dynamic and static ones (of course such a division is rather artificial). The static effects include the ΔE-effect (investigated by dynamic methods), the spontaneous symmetry breaking (discussed in the reviews of Refs. 1 and 2), and some other effects. This paper deals with the following dynamic effects: rotation of the plane of polarization, acoustical birefringence and magnetoacoustical resonance (MAR). MAR was theoretically predicted in the mid-50's (Refs. 3–5). Sound wave attenuation increases considerably at resonant conditions with the spin wave[1)] (when their frequencies and wave vectors coincide). It is a rather rare case in acoustics of a resonant response of a medium. The acoustical nuclear resonance and other quantum acoustics effects in which the medium can be represented, for example, by a two-level system can also be regarded as the same type of phenomena. We note that MAR is connected with electron spins. The coupling of phonon and magnon subsystems is a weak one, as a rule. Nevertheless, under MAR conditions this coupling increases drastically. On the other hand, in high-quality ferrodielectric crystals due to the high-Q property of spin precession magnon excitations have a long lifetime and can considerably affect the phonon excitations even in the case of weak coupling. The high mobility and great nonlinearity of the magnetic subsystem have a big influence upon the acoustical characteristics of such materials even under nonresonant conditions (when magnetic relaxation occurs). External magnetic fields can be used to control the relaxation times and other characteristics. Magnetoacoustic spectroscopy leads to a better understanding of different kinetic processes in magnetic materials. Several reviews include some aspects of MAR investigations. [Refs. 2, 7–12].

In this paper we have made an attempt not only to summarize the main experimental and theoretical results but also to discuss some new effects. The latter include MAR line broadening in inhomogeneous internal fields, fine structure of MAR spectra, and nonlinear effects at resonance.

An intensive search for different types of materials with high effective nonlinearity was made recently. Such materials provide an opportunity for various applications in sensors and acoustoelectronic signal processing devices. An effect of exchange increase of acoustic nonlinearity by 3–4 orders of magnitude was discovered in antiferromagnetics.[13] The magnetoelastic nonlinearity of yttrium-iron garnet (YIG)-type ferrites increases more than by five orders of magnitude in the MAR region. The discovery of powder and domain echo in polycrystals and long-term memory in ferrites[14,15] opens up new prospects for applications.

It should be noted that magnetoacoustic resonance and magnetoacoustic spectroscopy are very powerful experimental tools. They can be of great help in the investigation of different magnetic characteristics: internal magnetic field, domain structure, spin-spin and spin-lattice relaxation times, etc. It must be said that the number of papers on magnetoacoustics is very limited in spite of obvious application opportunities. The aim of this paper is to present a systematic review of these publications.

1. THE THEORY OF SPIN-PHONON INTERACTION AND MAGNETOACOUSTIC RESONANCE

Both quantum and phenomenological approaches can be applied to the theoretical analysis of magnetoelastic wave propagation. The first one was developed in Ref. 16 and used Hamiltonian formalism to describe resonance interaction of spin and elastic waves. In spite of the greater generality of such an approach it is often more convenient to use the phenomenological one. Using it we can obtain practically all the important results with greater clarity and simplicity. It should be pointed out that, as far as we know there is still no absolutely complete spin-phonon interaction theory which takes into account such effects as crystal anisotropy, domain structure, special features of internal fields and their inhomogeneity, and dissipative properties of crystals. A simple theory of magnetoelastic wave propagation is given, for example, in Ref. 9. It doesn't allow for internal field nonuniformity that has, in fact, a substantial bearing on all the magnetoelastic wave features, the resonant frequencies, MAR

 0038-5670/92/020106-17$03.00

profile, etc. Here we shall present theoretical results on the interaction of longitudinal (L) and shear (S) waves with the spin-system of a cubic ferromagnetic crystal. Due attention will be paid to the demagnetizing field nonuniformity: this field in monodomain approximation has the highest value among all relativistic internal fields of typical magnetic crystals (YIG, spinels).

The thermodynamic potential of a magnetic substance can be presented in the form:[1,9,17]

$$\Phi = \Phi_e + \Phi_{me} + \Phi_m \tag{1.1}$$

where Φ_e is the elastic, Φ_{me}—magnetoelastic and Φ_m—magnetic parts of the potential. The system of magnetoelasticity equations is:[1,9]

$$\rho \dot{U}_i = \frac{\delta}{\partial x_j} \frac{\delta \Phi}{\delta U_{ij}} \frac{1+\delta_{ij}}{2}, \tag{1.2}$$

$$\dot{\mathbf{m}} = \gamma \left[\mathbf{m} \frac{\delta \Phi}{\delta \mathbf{m}} \right]; \tag{1.3}$$

where $\mathbf{m}$ is a unit magnetization vector, U_{ij}—are the components of the strain tensor, γ—is the gyromagnetic ratio for the electron spin, δ_{ij}—is the Kronecker delta symbol, and ρ is the density of the material. The effective magnetic field $\delta\Phi/\delta\mathbf{m} = -\mathbf{H}_{\text{eff}}$ is the vector sum of the external field $\mathbf{H}_0$ and the internal field $\mathbf{H}_{\text{in}}$. The latter is the sum of the anisotropy field $\mathbf{H}_a$, the dipole-dipole interaction field $\mathbf{H}_d$ (the demagnetizing field) and the exchange field $\mathbf{H}_e$. The Bloch–Landau equations (1.3) are written in the dissipationless approximation. Equations (1.2) and (1.3) are coupled and essentially nonlinear. The basic nonlinearity is of magnetic nature. The lattice nonlinearity is small compared to it so we can neglect it and use only the first term of the Φ_e expansion. Eqs. (1.2–1.3) can be solved by the successive approximations method for small strains and small deflections of the magnetization vector from its equilibrium state $\mathbf{m}_0$. In the linear approximation this system had been solved for the simple crystallographic classes of magnetic materials with uniform effective magnetic fields (for example, in Ref. 1). The cases of polydomain crystals and samples with nonellipsoidal shape had not been analyzed; meanwhile these cases are of interest for application purposes.

Let us consider magnetoelastic waves in magnetic materials with an inhomogeneous demagnetizing field. The latter can be written as $\mathbf{H}_d = -4\pi \mathbf{M}_0 f(x,y,z) \hat{N}$, where $\mathbf{M}_0$ is the saturation magnetization, $f(x,y,z)$ describes internal field distribution and can be derived from magnetostatic equations; $\hat{N}$ is the demagnetization tensor. If $\hat{N}$ has only diagonal terms then $H_{di} = -\sigma m_i N_{ii}$ where $\sigma = 4\pi M_0 f$ and m_i are the components of $\mathbf{m}$ ($i = x,y,z$). Using Eq. (1.3) we can obtain the equilibrium equations for $\mathbf{m}^0$ if $\mathbf{H}_0$ is directed along z ($i = x,y$):

$$m_i^0 \left[H_0 - [2K_1/M_0 m_z^0 (m_i^{02} - m_z^{02})] - \sigma m_z^0 \Delta_{zi} \right] = 0,$$

$$m_x^0 m_y^0 \left\{ \sigma \Delta_{xy} - [2K_1/M_0 (m_x^{02} - m_y^{02})] \right\} = 0, \tag{1.4}$$

where K_1 is the anisotropy coefficient; $\Delta_{pk} = N_p - N_k$.

For $H_0 = 0$ the solutions of Eq. (1.4) are presented in Table I. It must be noted that taking $\mathbf{H}_d$ into account had no effect on the [100] type equilibrium directions but did change the [111] type directions.

The solution (1.5) corresponds to the case of magnetic saturation in the absence of an external field. This case was analyzed in detail earlier[9,12,18] and here are the main results. Under condition of cylindrical symmetry $N_x = N_y$ and if the angle $(\mathbf{H}_0,\mathbf{k}) = \theta = 0°$ ($\mathbf{k}$ is the wave vector of the magnetoelastic wave) the solution of Eqs. (1.2–1.3) indicates that the longitudinal wave propagating along z does not interact with the magnetic subsystem. The coupling occurs only for one of two circularly-polarized shear waves.[19] This wave has the clockwise polarization (polarization vector rotates clockwise with respect to the $\mathbf{k}$ direction). The dispersion relation[8,9,2)] for this wave is

$$\omega/\gamma = M_0 B_2^2 k^2 (\rho\omega^2 - k^2 C_{44}) + 2Ak^2 - \sigma\Delta_{zx} + H_0, \tag{1.9}$$

where B_2 is the second magnetoelastic constant, C_{44} is the modulus of elasticity and A is the exchange constant. These results are close to those obtained in Ref. 9 after correction for the demagnetizing field. A similar dispersion relation for different angles θ can be found in Ref. 20. The dispersion curves of elastic and spin waves are shown in Fig. 1. The elastic wave dispersion relation is ω-kV (where V is the sound velocity). The spin waves dispersion relation neglecting anisotropy is:[7,10,12]

$$\omega_c = \gamma [(H_{\text{eff}} + Ak_c^2)(H_{\text{eff}} + 4\pi M_0 \sin^2\theta_c + Ak_c^2)]^{1/2}, \tag{1.10}$$

where ω_s, k_s and θ_s are, respectively, the frequency, the wave number of the spin wave and the angle between its direction of propagation and $\mathbf{H}_0$.

1.1. Shear waves

Resonance usually appears in the region of dispersion curves crossover. Magnetoelastic coupling of the shear

TABLE I. Equilibrium directions of the magnetization vector ($\chi = \sigma M_0/2K_1$).

m_x^0	m_y^0	m_z^0	Eq. No.
0	0	± 1	(1.5)
± 1	0	0	(1.6)
0	± 1	0	(1.7)
$+\frac{1}{\sqrt{3}}[1-\chi(\Delta_{yz}+\Delta_{zx})]^{1/2}$	$+\frac{1}{\sqrt{3}}[1-\chi(\Delta_{xy}+\Delta_{zy})]^{1/2}$	$+\frac{1}{\sqrt{3}}[1-\chi(\Delta_{xz}+\Delta_{yz})]^{1/2}$	(1.8)

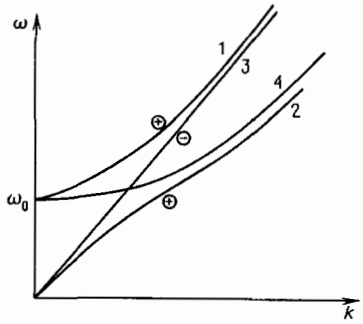

FIG. 1. Dispersion curves: *1,2*—magnetoelastic waves propagating along the magnetic field direction ("+"—clockwise and "−"—counter-clockwise circularly polarized waves), *3*—unperturbed elastic and *4*–unperturbed spin waves.

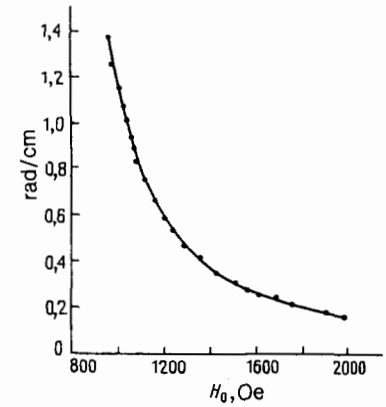

FIG. 2. Rotation per unit length as a function of the applied magnetic field in YIG.[21]

waves propagating in the [100] direction occurs for all θ and reaches its maximum at $\theta = 0°$.[20] A wave with linear polarization can be represented by two circularly polarized waves with opposite directions of rotation. It was already pointed out that only one of them interacts with the spin system under such conditions. In this case the velocities of these two components become different. This leads to the phenomenon of the polarization plane rotation (also called the acoustical Faraday effect). The rotation angle per unit path length was derived in Refs. 9, 21. The wave numbers of clockwise (k^+) and counter-clockwise (k^-) polarized waves are described by the following equation:

$$(k^{\pm})^2 = \frac{\omega^2}{V_t^2}\left\{1 + \frac{\gamma b_2^2}{YM_0\rho V_t^2[(\omega^2/V_t^2) - (-\gamma H_0 \pm \omega)Y^{-1}]}\right\}, \tag{1.11}$$

where V_t is the transverse waves velocity, $Y = 2A\gamma/M_0$, $b_2 = B_2 M_0$. For small k the specific rotation of the plane of polarization is

$$\frac{\varphi}{l} = \frac{1}{2}(k^+ - k^-) = -\frac{\gamma b_2^2\omega^2}{2M_0\rho V_t^3(\omega^2 - \gamma^2 H_0^2)}. \tag{1.12}$$

Fig. 2 presents the characteristic specific rotation as a function of the applied external magnetic field. According to Eq. (1.12) φ/l sharply increases in the resonance region when H_{eff} approaches ω/γ. The more complete theory of S-waves coupling with the spin waves along three main directions of propagation was considered in Refs. 10, 22. Only one circularly polarized wave is coupled with the spin-system for [100] and [111] directions at $\theta = 0°$. At $\theta = 45°$ magnetoelastic coupling exists only for the shear wave with transverse polarization and at $\theta = 90°$ for a wave with polarization lying in the plane including $\mathbf{H}_0$ and $\mathbf{k}$. In the [110] direction magnetoelastic coupling exists at $\theta = 0°$ for all elastic waves and at $\theta = 90°$ for the shear waves with polarization parallel to the applied magnetic field.

As has been already pointed out the solution $m_x^0 = m_y^0 = 0; m_z^0 = 1$ is valid only for a cylinder-like sample magnetized to saturation. The condition of cylindrical symmetry represents a geometrical restriction for most acoustic applications. Another possible solution of equilibrium equations is (1.8). The magnetoelastic wave propagation problem during the magnetization process is very complicated in this case and can be solved only numerically.

The third solution is either $m_x^0 = 0$ (1.7) or $m_y^0 = 0$ (1.6). This case was treated in detail in [23]. We can ignore the exchange and the anisotropy fields. The first one makes an essential contribution to internal field only at very high frequencies and the second one usually is much smaller than the demagnetizing field.

Let us first consider the shear magnetoelastic wave propagating along [001] and, hence, along $\mathbf{H}_0$. Unlike [9] we shall assume here that the equilibrium magnetization satisfies the (1.7) condition. This will help us to take into account probable processes of rotation. After applying the external magnetic field the equilibrium values of the unit magnetization vector can be derived from Eq. (1.4) and have the form

$$m_x^0 = 0, \quad m_y^0 = \pm(\sigma^2\Delta_{zy}^2 - H_0^2)^{1/2}/\sigma\Delta_{zy}, \quad m_z^0 = H_0/\sigma\Delta_{zy}. \tag{1.13}$$

The magnetoelasticity equations yield elastic constant renormalization due to the magnetoelastic coupling:

$$C_{44}^{\text{eff}} = C_{44} + \frac{M_0 B_2^2 H_0^2 \omega_0^2}{3\sigma\Delta_{zy}^2\Delta_{yx}(\omega_0^2 - \omega^2)}, \tag{1.14}$$

here ω_0 is the magnetic moment precession frequency:

$$\omega_0^2 = \gamma^2(H_0^2 - \sigma^2\Delta_{zy}^2)\Delta_{yx}/\Delta_{zy}. \tag{1.15}$$

The shear wave velocity can be derived from Eq. (1.15) in terms of H_0:

$$V_s^2 = \frac{C_{44}}{\rho} + \frac{M_0 b_2^2 H_0^2}{\rho\sigma^3\Delta_{zy}^2\Delta_{yx}} + \frac{M_0 B_2^2 H_0^2 \omega^2}{\gamma^2\rho\sigma^3\Delta_{zy}\Delta_{yx}^2[H_0^2 - \sigma^2\Delta_{zy}^2 - (\Delta_{zy}\omega^2/\Delta_{yx}\gamma^2)]}. \tag{1.16}$$

The coupling of the elastic and magnetic subsystems causes the dispersion of the sound velocity. The resonant interaction of the sound wave with the spin-system is possible for relatively low frequencies $\omega \ll \gamma H_0$ and long thin samples as can be seen from Eq. (1.15). This phenomenon is called S-MAR (shear wave MAR).

The case of $m_y^0 = 0$ can be treated by analogy. The equilibrium components of $\mathbf{m}^0$ are:

$$m_x^0 = \pm (\sigma^2\Delta_{zx}^2 - H_0^2)^{1/2}/\sigma\Delta_{zx}, \quad m_z^0 = H_0/\sigma\Delta_{zx} \quad (1.17)$$

and the free spin wave dispersion relation is:

$$\omega_0^2 = \gamma^2(\sigma^2\Delta_{zx}^2 - H_0^2)\Delta_{xy}/\Delta_{xz}. \quad (1.18)$$

1.2. Longitudinal waves

Now we shall discuss the resonance of longitudinal waves (L-MAR) in a single domain cubic crystal. Eqs. (1.3) show that an alternating magnetic field component perpendicular to the constant external field is needed to excite the spin-system. Unlike Ref. 24 in Ref. 7 it was shown that an L-wave propagating in all three main directions is accompanied by a longitudinal alternating magnetic field. In the [110] direction however this field has a small addition of a transverse component. The longitudinal character of the alternating field makes it impossible to observe L-MAR at $\theta = 0°$ Refs. 9, 10, 16, 20, 22, 24, 25. Nevertheless the resonance occurs at $\theta = 90°$. It must be noted that the authors of Refs. 9, 16, 18, 20 deny the possibility of such an observation for [100] and [111] directions and according to Refs. 10, 24 MAR in the [110] direction exists only in case of magnetoelastic isotropy ($2B_1 = B_2$). The magnetoelastic interaction problem for cubic crystals was solved in Ref. 26 for the case (1.17) in presence of smooth variations of the internal field. Let us consider L-wave propagation along the [100] direction

$$\frac{\partial U_x}{\partial x} = U_0\cos(\omega t - kx). \quad (1.19)$$

in the presence of an external field directed along [001]. The spin precession stimulated by the accompanying magnetic field can be obtained from the first approximation of the Bloch–Landau equation (1.3):

$$\begin{aligned} m_x' &= (\gamma^2 H_0 m_x^0 \Delta_{xy}/\Delta_{zx})\Lambda\cos(\omega t - kx), \\ m_y' &= \gamma\omega m_x^0 \Lambda\sin(\omega t - kx), \\ m_z' &= (\omega^2/\sigma\Delta_{zx})\Lambda\cos(\omega t - kx), \end{aligned} \quad (1.20)$$

where $\Lambda = 2B_1 m_z^0 U_0/(\omega_0^2 - \omega^2)$, and ω_0 is determined by the relation (1.8). The primary magnetization is orthogonal to $\mathbf{H}_0$ according to (1.17). L-MAR occurs when the magnetic moment turns from this direction to that of external field according to Eqs. (1.17)–(1.18). This condition is satisfied when the magnetic moment is locally magnetized to saturation. We must stress that in the presence of a nonuniform magnetic field this is a locally fulfilled condition. The stimulated spin wave is such that the magnetic moment end moves along the surface of an ellipsoid defined by (1.20). For a low-frequency resonance this ellipsoid is very prolate along the direction of sound propagation.

We can write the renormalized L-wave velocity in the form

$$V_L^2 = (C_1/\rho) - \{2B_1^2 M_0 H_0^2 \omega_0^2/[(\omega_0^2 - \omega^2)\rho\sigma^3\Delta_{zx}^3]\}. \quad (1.21)$$

1.3. Nonlinear MAR

The linear S- and L-MAR theory in a magnetic material without losses had been presented above. The initial theory restrictions do not allow one to obtain one of the main MAR effects—the sharp increase of the sound wave absorption at resonance conditions. Nevertheless, most other significant features were illustrated: they include magnetoactivity of elastic waves, the rotation processes preceding the resonance and the sound velocity dependence on the external magnetic field. The nonlinear MAR also has a number of features that can be described in the dissipationless approximation to the Bloch–Landau equation (1.3).

One of the first theoretical papers on nonlinear magnetoelastic waves is Ref. 27. To describe the changes in magnetization brought about by an elastic wave in an isotropic ferrite it uses not the Bloch–Landau equations, but the equations of magnetostatics. This leads to the exclusion of the possibility of investigating the resonance interaction of sound with a magnetic subsystem. According to the estimates made in that paper due to the interaction of the longitudinal wave with the magnetic subsystem the quadratic nonlinear parameter (in the case when there is no magnetoelastic coupling that is in order of magnitude equal to the ratio of the elastic moduli of third order to the corresponding moduli of the second order) is proportional to M_0 and increases in the case of ferrites by more than an order of magnitude. From this one can conclude that in magnetic phase transitions (transition to a magnetically ordered phase, a spin-reorientation transition) the nonlinear parameter experiences a big change after the transition. However in the experimental investigations of Refs. 28, 29 no such significant change in the effective quadratic nonlinearity accompanying a transition to a magnetically ordered phase and a spin-reorientation transition in gadolinium and in a transition to the paraphase in terbium was observed. In Ref. 27 an erroneous conclusion was drawn concerning the impossibility of generating a transverse second harmonic by a transverse wave.

The second approximation of Eqs. (1.2) and (1.3) was solved in Ref. 26 for a longitudinal wave under the conditions (1.17). The second harmonic amplitude is

$$A_{2\omega} = \frac{\gamma^2 B_1^3 M_0^2 \Delta_{xy} k U_0^2 [4\gamma^2 H_0 \omega^2 (m_x^0)^4 q + \omega_0^2 (m_z^0)^4]}{(\omega_0^2 - \omega^2)\Delta_{zx}}, \quad (1.22)$$

where

$$q \approx \frac{(C_{11}k^2 - \omega^2\rho)(\omega_0^2 - \omega^2)H_0 + \gamma^3 H_0 \sigma^2 (m_z^0)^2 \Delta_{xy}^2 - 4\gamma^2 B_1^2 M_0 \sigma^2 (m_z^0)^5 \Delta_{xy}^2 k^2}{(\omega^2\rho - C_{11}k^2)(4\omega^2 - \omega_0^2)}. \quad (1.23)$$

The second harmonic resonance (nonlinear MAR) can be obtained at two frequencies $\omega_{01} = \omega$ and $\omega_{02} = 2\omega$ and, hence, according to (1.9) at two values of H_0. Such a doublet was first observed in Ref. 30. For a thin rod elongated in the x-direction ($\Delta_{zx}/\Delta_{yx} \approx 1; \Delta_{yx} \approx \Delta_{zx} \approx 1$) at low frequencies ($H_0^2 \approx \sigma^2 \gg H_{\rm eff}^2$) the doublet splitting is

$$\Delta H_\delta \approx 3\omega_0^2[1 + (5\omega_0^2/4\gamma^2\sigma^2)]/2\gamma^2\sigma, \tag{1.24}$$

This indicates that for LF MAR this doublet becomes hardly resolvable.

The results for the shear wave under the initial conditions (1.13) can be expressed in analogous form

$$A_{2\omega} = \frac{kB_2M_0\{qm_z^0 + [\gamma B_2^2\omega\omega_0^2 m_y^0(m_z^0)^2U_0/2\sigma\Delta_{yx}(\omega_0^2 - \omega^2)]\}}{2(\rho\omega^2 - C_{44}k^2)}, \tag{1.25}$$

where U_0 stands for the shear wave deformation amplitude and q is the second approximation of the magnetic moment m_x'':

$$\begin{aligned} q = {} & \gamma^3\sigma B_2^2\Delta_{zy}m_y^0m_z^0\omega U_0^2\{4(C_{44}k^2 - \omega^2\rho) \\ & \times [(2\omega^2 + \omega_0^2)(m_z^0)^2 + \omega^2 - \omega_0^2] \\ & + \gamma^2B_2^2M_0^2(m_z^0)^2(m_y^0)^4\Delta_{zy}k^2\} \\ & \times (1/2)(\omega_0^2 - \omega^2)^{-2}\{4\omega^2(\omega^2\rho - C_{44}k^2) \\ & - \omega_0^2[\omega^2\rho - k^2(C_{44} + M_0B_2^2(m_z^0)^2/\sigma\Delta_{yz})]\}^{-1}. \end{aligned} \tag{1.26}$$

We are interested mainly in the resonant behavior of m_x'' (and $A_{2\omega}$ accordingly). Estimates show that the last term in the square brackets of expression (1.26) is negligible. Then the denominator of (1.25) can be written in the following form:

$$(\omega_0^2 - \omega^2)^2(4\omega^2 - \omega_0^2)(\omega^2\rho - C_{44}k^2). \tag{1.27}$$

The second harmonic resonance of the magnetic moment (and $A_{2\omega}$, accordingly) can be observed in two cases: when the precession frequency ω_0 coincides with that of the sound wave and when it coincides with twice the sound frequency. The resonance conditions are fulfilled for two different values of H_0:

$$H_{\rm p1}^2 = \sigma^2\Delta_{zy}^2 + (\Delta_{zy}\omega_0^2/\Delta_{yx}\gamma^2),$$

$$H_{\rm p2}^2 = \sigma^2\Delta_{zy}^2 + (\Delta_{zy}4\omega_0^2/\Delta_{yx}\gamma^2). \tag{1.28}$$

The field doublet then is

$$\Delta H_\delta = 3\omega_0^2\Delta_{zy}/\gamma^2\Delta_{yx}(H_{\rm p1} + H_{\rm p2}). \tag{1.29}$$

For the case of relatively low frequencies $\omega \ll \gamma\sigma(\Delta_{zy}\Delta_{yx})^{1/2}$ we can assume $H_{r1} \approx H_{r2}$ and then

$$\Delta H_\delta \approx 3\omega_0^2/2\gamma^2\sigma\Delta_{yx}, \tag{1.30}$$

This expression is in agreement with (1.24) up to the demagnetizing Δ_{yx} correction. An effective gyromagnetic ratio γ^* (determined by the condition $\Delta H_\delta = \omega_0/\gamma^*$) is

$$\gamma^* = 2\gamma^2\sigma\Delta_{yx}/3\omega_0. \tag{1.31}$$

The expression γ^*/γ is of the order of the ratio of the demagnetizing field to the effective field if there is no cylindrical symmetry. In LF-MAR region γ^* has a high value and the doublet is hardly resolvable. For the same reason it is difficult to identify the MAR phenomenon by the shift of the resonance line as the sound frequency is varied.

Summing up we must say that the results presented in this section were obtained for a somewhat simplified model of a magnetic material. The theory was given essentially for a single-domain sample, with an inhomogeneous internal field in a dissipationless approximation. The magnetization of the sample was restricted to rotation processes, nevertheless even such a simple model has made it possible to discuss a number of MAR features. According to Eqs. (1.17) and (1.13), (1.18) and (1.15) LF MAR is observed in the regions where the magnetic moment is collinear with the external magnetic field. A rather high sound velocity dispersion arises at MAR conditions (see Eqs. (1.21) and (1.16)). A second harmonic doublet is hardly resolvable at low frequencies according to Eqs. (1.22) and (1.25). The effective magnetoelastic coupling constant: B_1 for L-waves (Eq. (1.21)) and B_2 for S-waves (Eq. (1.16)) increases sharply at resonance. This is accompanied by a great resonance-type increase in the second harmonic generation efficiency. Of course this increase and the sound velocity dispersion are limited by the dissipation processes that were not taken into account in our discussion. It is also pertinent to mention the "geometrical" difference of S-MAR and L-MAR. The best condition for the former is $\mathbf{H}_0 \| \mathbf{k}$, and for the latter $-\mathbf{H}_0 \perp \mathbf{k}$.

2. CONDITIONS FOR THE EXCITATION OF MAR AND LINE PROFILES IN MAGNETIC MATERIALS WITH INHOMOGENEOUS INTERNAL FIELDS

We will examine in greater detail the local conditions for MAR (Refs. 31, 32). Simple physical considerations allow qualitatively for the dissipation losses. According to the Bloch–Landau equation (1.3), the spin precession occurs around the direction of the effective field $\mathbf{H}_{\rm eff}$, which is generally a vector sum of the external $\mathbf{H}_0$ and the internal field $\mathbf{H}_{\rm in}$. The latter, as we have already noted, is the sum of the exchange and all the relativistic fields:

$$\mathbf{H}_{\rm eff} = \mathbf{n}f/\gamma = \mathbf{H}_0 + \mathbf{H}_{\rm in}, \tag{2.1}$$

where $\mathbf{n}$ is a unit vector and f is the resonance frequency. A resonance occurs if the oscillating magnetic field $\mathbf{h}$ created by the sound wave through magnetostriction is not parallel to the effective field: $[\mathbf{h} \times \mathbf{H}_{\rm eff}] \neq 0$. We shall assume that this condition is satisfied.

If f/γ has a fixed value and determines the radius of the sphere of possible values of $\mathbf{H}_{\rm eff}$ (Fig. 3), it is obvious that the disorientation angle $\beta = (\mathbf{H}_0, \mathbf{H}_{\rm in})$ can be found from

$$\sin\beta = \frac{1}{2H_0H_{\rm in}}\left[2\frac{f^2}{\gamma^2}(H_0^2 + H_{\rm in}^2) - \frac{f^4}{\gamma^4} - (H_0^2 - H_{\rm in}^2)^2\right]^{1/2}. \tag{2.2}$$

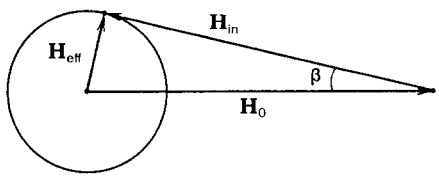

FIG. 3. Vector diagram of formation of the effective field in magnetic [32].

In a strongly magnetized crystal ($H_0 \gg H_{in}$) $f = \gamma|H_0|$ (microwave MAR), the collinearity of the external and the internal fields follows automatically from Eq. (2.2): $\beta = 0$. However, at frequencies $f \approx 10^8$–10^{10} Hz a resonance is observed in average fields $H_0 > H_{in}$ and the maximum permissible angle between fields can be found from

$$\sin\beta_{max} = f/\gamma H_0, \tag{2.3}$$

i.e. β_{max} increases with frequency. At LF-MAR conditions we have $|H_0| \approx |\mathbf{H}_{in}| \gg f/\gamma$, the angle β_{max} is small and we find from Eq. (2.2) that $f/\gamma = \pm(H_0 \pm H_{in})$. Out of these four solutions only $f/\gamma = \pm(H_0 - H_{in})$ have a physical meaning and, consequently, apart from the small resonance field, by analogy with Eqs. (1.18) and (1.15), we have

$$\mathbf{H}_0 \approx -\mathbf{H}_{in}. \tag{2.4}$$

In other words, the conditions of LF MAR are satisfied when the internal and the external fields have the same value. In contrast to the widely used magnetic methods of the sample average magnetization determination, MAR makes it possible to determine the local internal field.

If a shear wave propagates along the [001] axis parallel to the external magnetic field, then the magnetoelastic coupling occurs and $[\mathbf{h}\mathbf{H}_{eff}] \neq 0$. The internal field of a thin long crystal can be assumed as one-dimensional, i.e. $H_{in} = H_{in}(z)$. In this case the resonance occurs sequentially in different regions of the crystal: first at the center where $z = 0$ and $|\mathbf{H}_{in}|$ has a minimum value, then at $H_{in}(z) = H_{in}(-z)$ in regions symmetric with respect to the center and, last, near the ends of the crystal. In other words the structure of the internal field is scanned by the intrinsic ferromagnetic resonance line of width ΔH_i (caused by spin-spin and spin-lattice relaxation times under conditions of a uniform internal field). In this case we can determine the size δz of the resonance region and the MAR profile by the known function $H_{in}(z)$. Conversely, we can use the experimental shape of the profile to find $H_{in}(z)$. Because of the approximate equality given by Eq. (2.4) we shall ignore the difference between H_0 and H_{in}. The size δz corresponding to a small width ΔH_i can clearly be found from the expansion

$$\Delta H_i = H(z) - H(z + \delta z) = -H'\delta z - (1/2)H''\delta z^2 - \ldots \tag{2.5}$$

Outside the extrema and the inflexion points of the field we have

$$\delta z = -\Delta H_i/H'. \tag{2.6}$$

At field extrema

$$\delta z = (-2\Delta H_i/H'')^{1/2} \approx r_0(\Delta H_i/H^*)^{1/2}, \tag{2.7}$$

where H^* and r_0 are the characteristic local field and its range. The relationships (2.6) and (2.7) determine the local nature of the resonance. If the width ΔH_i is sufficiently small then the resolution of such a magnetoacoustic scanning can be rather high. The derivatives H' and H'' can be determined approximately from the experimental MAR profile, but an estimate of δz can be carried out by a more convenient way. In the case of a model parabolical field $H_{in}(z) = -H_{in}(0) - \alpha z^2$, (where $0 \leqslant z \leqslant L/2$ and L is the crystal length) the size of the resonance region outside the extrema and inflection points is given by the relation

$$\delta z = (L^2/8z)\Delta H_i/\Delta H, \tag{2.8}$$

whereas at the extrema we have

$$\delta z = (1/2)L(H_i/\Delta H)^{1/2}, \tag{2.9}$$

where $\Delta H = |H_{in}(L/2) - H_{in}(0)|$ is the width of the MAR profile (Fig. 4). These expressions are approximate not only because they use a parabolical distribution of the internal field but also they do not allow for a real domain structure, crystal defects and other magnetic irregularities that have local internal fields with values above $H_{in}(L/2)$. All these factors lead to the blurring of the MAR profile.

A linear magnetoacoustic spectrum $A_\omega(H_0)$, where A_ω is the amplitude of an acoustic pulse transmitted through a crystal, is clearly governed by the relationship

$$A_\omega(H_0) = A_\omega(0)\exp(-2\Delta\alpha\delta z), \tag{2.10}$$

where $\Delta\alpha = \alpha_r - \alpha$; α_r and α are, respectively, the absorption coefficients of sound at the resonance and away from it. In the case of a nonlinear spectrum (at second harmonic) we shall temporarily ignore its doublet nature and assume that the nonlinear parameter at the resonance satisfies $\Gamma_r \gg \Gamma_0$ and also $\alpha_r \gg \alpha$. So in approximation of the quadratic frequency dependence of the absorption we obtain

$$A_{2\omega} \sim (\Gamma_r/\alpha_r)[\exp(-2\alpha_r\delta z) - \exp(-4\alpha_r\delta z)]. \tag{2.11}$$

If

$$2\alpha_r\,\delta z \ll 1, \tag{2.12}$$

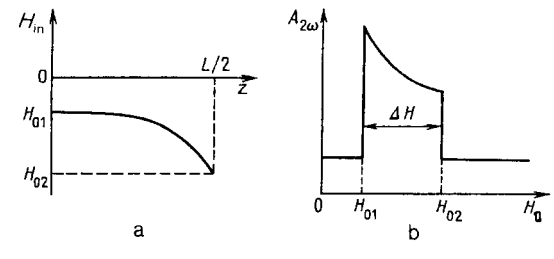

FIG. 4. A model distribution of the internal field (a) and the corresponding resonance profile of $A_{2\omega}(H_0)$—(b).

which is valid at least in regions with high internal field gradients according to Eq. (2.6). And so we find that

$$A_\omega(H_0) \sim -2\alpha_r \delta z, \quad A_{2\omega}(H_0) \sim 2\Gamma_r \delta z. \tag{2.13}$$

The absorption at the resonance is caused by the increase of the magnetoelastic coupling and effective energy dissipation in the magnetic subsystem. On the other hand, the mechanism of Γ_r increase is also due to resonant enhancement of the magnetoelastic coupling, the nonlinearity of this coupling and particularly the nonlinearity of the magnetic subsystem. It is qualitatively clear that all these factors should also increase the damping α_r.

The condition (2.12) may not be satisfied in the case of wide extrema of $H_{in}(z)$, particularly in the case of crystals with fairly strong magnetoelastic coupling, with a long spin precession relaxation time τ, and, consequently, with a strong resonant increase in absorption. The profile $A_\omega(H_0)$ then represents the distorted spectrum of $\alpha(H_0)$, and the profile $A_{2\omega}(H_0)$ represents the spectrum of $\Gamma(H_0)$. It is clear from Eq. (2.11) that these dissipative distortions begin to manifest themselves particularly strongly beyond the second harmonic stabilization length, i.e. when

$$2\alpha_r \delta z \geq 0{,}5 \ln 2 = 0{,}35. \tag{2.14}$$

The nonlinear absorption due to strong generation of higher harmonics of a magnetoelastic wave then begins to play the dominant role in the resonance region.

The relations (2.6), (2.7) and (2.10), (2.11) link the line profile with the field distribution. If $H_{in}(z)$ is given we can readily find the MAR profile from this relationship and, conversely, we can use $A_\omega(H_0)$ or $A_{2\omega}(H_0)$ to reconstruct $H_{in}(z)$. The first attempts to use the MAR phenomenon for internal field reconstruction were made in Refs. 32, 33. A unique reconstruction is possible only if the function $H_{in}(z)$ is single-valued in the $0 \leqslant z \leqslant L/2$ interval and provided $H_{in}(z) = H_{in}(-z)$. For example, Fig. 4a shows the characteristic distribution of $H_{in}(z)$ and the corresponding profile of $A_{2\omega}(H_0)$ (Fig. 4b). The MAR begins in a field H_{01} equal to the internal field $H_{in}(0)$ at the center of the crystal. Then $A_{2\omega}$ decreases in accordance with the variation of $H_{in}(z)$ and, finally, the MAR disappears at the boundary of the crystal in a field $H_{02} = H_{in}(L/2)$. The width of the profile is ΔH. This is the so-called canonical profile obtained in a given magnetic internal field $H_{in}(z)$ that does not vary in the course of magnetization. This profile is characteristic for relatively long prismatic and cylindrical samples commonly used in magnetoacoustic experiments. It follows from the above discussion and also from direct experiments that LF MAR occurs in fields slightly lower than the saturation magnetization fields. It means that resonance excitation occurs against the background of domain structure modification processes: domain walls displacement and magnetization vector rotation. In spite of this and the assumed one-dimensional nature of $H_{in}(z)$, measurements made on long and relatively thin ferrite samples under conditions of low dissipative distortion yield near-canonical profiles of the linear and nonlinear S-MAR in contrast to L-MAR: the profile has a sharp leading edge and characteristic asymmetry.

In some cases experiment shows that the polydomain nature of a crystal strongly affects the damping and eliminates the possibilities of LF MAR observation. In the saturation region domain damping disappears and the crystal becomes acoustically transparent, but the local magnetic fields exceed the resonance value at the selected relatively low frequency throughout the crystal.

The possibility of observing magnetically charged defects is of practical interest. Fairly strong inhomogeneous internal fields are likely to exist near defects. Therefore, resonance conditions in the region of a defect should be obtained in external fields exceeding the saturation field. However, in view of the short range r_0 and high value of H^* in Eq. (2.7), these regions have small effective dimensions δz and should be strongly smeared out in the magnetic spectrum $A_\omega(H_0)$. This masking of small high-field defects eliminates the opportunity of their position determination. The influence of such defects can be manifested only in the background magnetic absorption in the saturation region.

Naturally, the observation of MAR is possible only if

$$f\tau > 1, \tag{2.15}$$

where τ is the effective spin relaxation time. This condition limits both the MAR lower frequency and the class of the objects. The latter must be crystals with the intrinsic ferromagnetic resonance line width obeying

$$\Delta H_i < H_{eff} = f/\gamma. \tag{2.16}$$

In this connection it is worth mentioning certain difficulties of MAR observation. In the HF range we need crystals with low acoustic losses; on the other hand, observation of LF MAR requires not only this (though the class of crystals is extended) but also a narrow ferromagnetic line width. It should be noted that this line width depends upon the resonance frequency and is determined mostly by the spin-spin relaxation time. By the estimates of Ref. 34 the spin-precession quality factor $Q = H_{eff}/\Delta H_i$ of manganese-zinc spinel (MZS) single crystals has a constant value over the frequency range of 10^7–10^{10} Hz. It means that the intrinsic ferromagnetic line width decreases at low frequencies. This fact leads to an easier MAR observation and to a better resolution of the magnetoacoustic spectroscopy.

We shall end this section with an estimate of the resolvability of the nonlinear MAR doublet. The doublet is resolved under the obvious condition $\Delta H_\delta > \Delta H_i$, which gives

$$f\tau > H_0/H_{eff}. \tag{2.17}$$

This condition is more stringent than the condition for the MAR observation given by Eqs. (2.15), (2.16). At lower frequencies it ceases to be satisfied and the doublet is not resolved.

3. EXPERIMENTS

A number of experimental publications on the coupling of spin and acoustic waves has appeared over the last 30 years. The results of some of them are in contradiction not only with each other but also with theory. In this section we will try to discuss and analyze the main experimental results.

The first experiments[35–37] on magnetoelastic interaction had been performed in the late fifties. The parametric excitation of acoustic vibrations of a spherical yttrium-iron garnet (YIG) single crystal was investigated in Ref. 35. The sample was placed into an electromagnetic resonator cavity

and was magnetized by an external constant magnetic field. The resonator was excited at the frequency of 9 GHz. To study the mechanism of the resonance in detail additional experiments were made to confirm the acoustic nature of the resonance, including determination of the sample vibration eigenfrequencies and the change of its acoustic resistance. The conclusion was made that the parametric excitation of acoustic vibrations has a magnetostrictive nature.

An increase of the shear acoustic waves absorption was observed[36,37] at 1 GHz in monocrystalline YIG disks and thin (about 15 acoustic wavelengths) Ni films in a certain range of the external fields. The special feature of these experiments is the use of extremely small samples (the disks had a diameter equal to 0.3 cm and a thickness of 0.0125–0.03 cm). These conditions lead to a uniform spin precession interaction with low mode mechanical vibrations of the whole sample. The wave character of the resonant interaction had no essential influence. The sample shape provided a uniform internal field.

In 1962–1970 Luthi had carried out magnetoelastic coupling investigations using acoustic excitation of different crystals at frequencies of 50–150 MHz.[38–45] Table II pre-

TABLE II.

Reference	Wave type	f, MHz	Sample	Orientation of its long axis	Experimental arrangement	Observed effects and measured values ($[b]$ = erg/cm^3, $[v]$ = cm/sec)
16	S, L	100–1700	YIG	[100], [111]	$\theta = 0, 90°$	Rotation of the plane polarization, MAR
18	S	528	YIG	[100]	$\theta = 0$	Rotation of the plane polarization, $B_2 = 7.4 \cdot 10^6$
19	S, L	1000	YIG	[100], [110], [111]	$0<\theta<90$	MAR, $B_1 = 3.5 \cdot 10^6$, $B_2 = 6.5 \times 10^6$
23	L	30	MZS	[100], [110], [111]	$0<\theta<90$	Linear m/a spectra, NMAR(*), ang. depend. of NMAR
27	L	560	YIG	[100], [110], [111]	$\theta = 0$	NMAR
28	S	30	YIG	[100]	$\theta = 0$	MAR, NMAR
29	S	30	YIG, MZS	[100], [110], [111]	$\theta = 0$	MAR, NMAR
30	S	30	YIG, MZS	[100], [110]	$\theta = 0$	MAR, NMAR, field depend. of $A_{3\omega}(H_0)$
32	S	5–30	YIG	—	$\theta = 0$	MAR
34	S	1000	YIG	—	$\theta = 0$	Absorption of sound
35	S, L	50–150	YIG	—	$0<\theta<90°$	Rotation of the plane polarization, $B_2 = 19 \cdot 10^6$, MAR, Birefringence, $B_2 = 24 \cdot 10^6$, MAR
36	S, L	50–150	YIG, YGaIG	[100], [110]	$0<\theta<90°$	MAR
37	S, L	110	TbIG	—	$\theta = 90°$	MAR
38	S	50–200	GdIG	[100]	$\theta = 90°$	MAR, birefringence, $B_2 = 16 \cdot 10^7$
39	S, L	70–150	GdIG, YIG	—	$\theta = 90°$	MAR, birefringence
41	S	70–210	Ni, magnetite	—	$\theta = 90°$	Birefringence
43	S	500–1000	YIG	[100]	$\theta = 0$	Temperature dependence of sound damping
44	L	50–220	YIG	[110]	$0<\theta<90°$	MAR, $v = 7.15 \cdot 10^5$
45	L	221	YIG	[110]	$0<\theta<90°$	MAR, depend. of the damping factor on H_0
46	L	780	$RbNiF_3$	—	$\theta = 45°$	Depend. of the damping factor on H_0, T
47	S	820	YIG	[100]	$\theta = 0, 90°$	Rotation of the plane polarization ($B_2 = 7.2 \times 10^6$), MAR Birefringence ($B_2 = 6.8 \times 10^6$)
48	S	800	$RbNiF_3$	—	$\theta = 90°$	Birefringence, $v = 2.7 \cdot 10^5$
50	L	30	MZS	[100]	$\theta = 90°$	MAR, NMAR, ang. depend. of L-MAR
51	S, L	100–1700	YIG	[100], [110], [111] [113]	—	NMER
52	S	300–1800	YIG	[110], [111]	—	NMER
53	L	100–220	YIG	[110]	$0<\theta<90°$	MAR, $v = 7.15 \cdot 10^5$, $Q = 10^4$
54	L	600–900	YIG	[111], [351]	—	MAR
55	L	1000	YIG	[110]	$0<\theta<90°$	Interaction of spin and elastic waves
56	L	250–1800	YIG	[110]	$\theta = 90°$	MAR
57	S	540	YIG	[111]	$\theta = 90°$	Interaction of oppositely moving waves
58	S	30	YIG	[100]	$\theta = 0$	NMAR, $\Gamma(H_0)$
59	S	30	YIG	[100]	$\theta = 0, 30°, 45°, 54°$	MAR, NMAR
			MZS	[110]	$0<\theta<90°$	
60	S	30	MZS	[110]	$\theta = 0$	NMAR, depend. of $A_{2\omega}$ maximum on h
61	S	30	MZS	[100], [110], [111]	$\theta = 0$	MAR, NMAR
62	S	30	MZS	[100], [110], [111]	$\theta = 0$	MAR, NMAR, influence of m.f. inversion on m/a spectra
63	S	30	YIG	[100]	$\theta = 0$	2-d and 3-d ac harmonic generation, distortion of ultrasound wave form
64	S	30	YIG, MZS	[100], [110], [111]	$\theta = 0$	MAR, reconstruction of internal field
65	S	9420	YIG	[100]	$\theta = 0$	Magnetoelastic coupling

*NMAR denotes nonlinear MAR
*NMER denotes natural magneto-elastic resonance.

sents data on the investigated crystals, the experimental conditions and the results of most of the experiments discussed in our review. Luthi differentiates three fundamentally different types of magnetoelastic coupling:[42] 1) rotation of the shear wave polarization plane (an analog of the Faraday effect in magnetooptics); 2) acoustic birefringence; 3) magnetoacoustic resonance.

In spite of some arbitrariness of such a classification we shall use it and shall now discuss these phenomena in detail.

1. The effect of rotation of the wave polarization plane is manifested if the wave propagation direction is parallel to the external magnetic field. It was first observed in Ref. 21. It was shown in an earlier section that the shear wave can be represented by two circularly-polarized waves and in magnetoelastic media only one of them interacts with the spin-system.[7,19] This is the cause of the difference in the velocities of these two components which, in turn, leads to polarization plane rotation (Fig. 5). The pulse amplitudes oscillate as the magnetic field is varied. The oscillation period becomes shorter as resonance is approached and is governed by Eq. (1.12). The magnetoelastic coupling constant B_2 can be derived from the dependence of the specific rotation on the external magnetic field Refs. 10, 21, 22, 50. The direct experimental verification of interaction of spin waves with only one circularly-polarized component was conducted in Ref. 22. The methodological feature of this experiment is the use of Al-Y garnet plates of $\lambda/4$ thickness to convert the linearly-polarized wave into a circularly-polarized one.

2. Acoustical birefringence (an analog of the Cotton-Mouton magnetooptical effect) occurs when the shear waves propagate in a direction orthogonal to the magnetic field. One of the wave components with polarization $\mathbf{p}$ directed along $\mathbf{H}_0$ interacts with the magnetic subsystem: its velocity and attenuation change, especially at resonance. The second component with $\mathbf{p}\perp\mathbf{H}_0$ does not interact with the spin-system. A wave with initial polarization, for example, $(\mathbf{p},\mathbf{H}_0) = 45°$ (Ref. 42) will change its polarization in the course of propagation due to the fact that these two components have different phases in the different regions of the sample. If this phase shift $\Delta\phi$ is equal to $\pi/2$ then the wave polarization becomes a clockwise-rotating one. Then as the phase shift increases to π the wave becomes once more a linearly-polarized one with $(\mathbf{p},\mathbf{H}_0) = 135°$. The subsequent increase of $\Delta\phi$ up to $3\pi/2$ and 2π leads to counter-clockwise rotation of the polarization and to initial wave polarization respectively. An analogous change of polarization of the acoustic wave transmitted through the crystal can be observed as the external magnetic field is varied. If we use a linearly-polarized receiving transducer we shall see a sequence of maxima and minima of amplitude as a function of $\mathbf{H}_0$ (as illustrated in Fig. 6). The birefringence phenomenon was investigated in Refs. 38, 41, 42, 44, 50, 51 using crystals with different structure (see Table II).

3. Magnetoacoustic resonance represents synchronous interaction of spin and acoustic waves in a certain range of magnetic field and is manifested by a strong increase in the absorption of the latter wave. Moreover, as has been pointed out, S-MAR can be detected by the increase of the polarization plane rotation frequency and by the increase of the frequency of oscillations under the acoustic birefringence conditions. Thus we can obtain information about the resonant interaction of spin and elastic subsystems from all three of the discussed phenomena. It must be noted that the authors of some papers on magnetoelastic interactions named parametric resonance as MAR. For example, parametric excitation of magnetoelastic waves by longitudinal magnetic pumping was investigated in Ref. 25 and parametric excitation of two spin waves by an elastic wave in Ref. 52. These phenomena will not be discussed in this paper.

We shall now consider in detail magnetoacoustic resonance using acoustic excitation. S-MAR was observed in Refs. 38, 39, 41 in different garnet samples (unfortunately with unknown orientation) in transverse magnetic fields under $\mathbf{p}\|\mathbf{H}_0$ condition. It should be pointed out that according

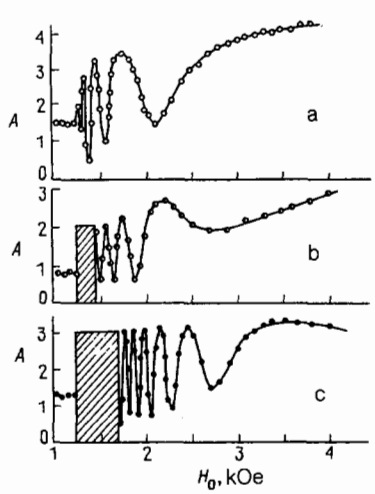

FIG. 5. Dependence of acoustic pulse amplitude on the external magnetic field (shear wave propagates along magnetic field direction in a YIG single crystal). a–c—the second, the fourth and the sixteenth pulses respectively. The ranges of very rapid pulse oscillations are shaded. $f = 820$ MHz.[50]

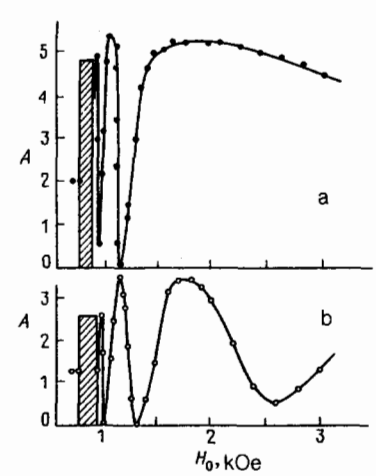

FIG. 6. Dependence of acoustic pulse amplitude on the external magnetic field for shear waves propagation perpendicular to H_0 in a YIG single crystal. $\theta = 45°$. a,b—the second and the fourth pulses respectively. $f = 1580$ MHz.[50]

to the theory presented above LF MAR can not be observed under such experimental conditions.

The first observation of L-MAR was conducted in Ref. 38. The magnetoelastic coupling was found to have a maximum value at $\theta = 17°$ and to be zero at $\theta = 0°$ and 90°. We must note that there are many contradictions in L-MAR results mostly concerning the θ-dependence. The most complete, from our point of view, theoretical analysis of L-MAR and the results of experiments on it are given in Refs. 26, 34, 53. We shall discuss these results in detail later.

Resonance absorption of elastic waves can be observed in the equivalent fields of magnetocrystallographic anisotropy even in the absence of an external field. This phenomenon called natural magnetoelastic resonance (NMER) was investigated in Refs. 51, 52 and is demonstrated in Fig. 7. The sharp peaks of shear wave absorption in YIG crystals disappear above the Curie temperature and in strong magnetic fields at room temperature. This leads to the conclusion of magnetic nature of the absorption. An absorption maximum in a Ca-Bi-V-garnet crystal was observed at lower frequencies than in YIG crystals because of weaker anisotropy and a lower saturation magnetization of this material. The resonance absorption of elastic waves takes place when the spin and elastic wave frequencies are equal. From expression (1.10) for this frequency it follows that at $H_0 = 0$ the effective field still contains the magnetic anisotropy field term and the resonance can occur. In the absence of an external field the sample consists of magnetic domains with magnetization directed mostly along the easy magnetization axis [111]. So for the angle θ we must take all possible angles between [111] type directions and the sound wave direction. The resonance frequencies derived from Eq. (1.10) coincide closely with the experimental ones. The contribution of domains with magnetization direction essentially deviating from the easy magnetization axis to the elastic wave absorption was discussed in Ref. 54.

L-MAR in a YIG sample of [110] orientation was investigated in Ref. 53 at frequencies lying in the 100–200 MHz range under conditions of an inhomogeneous internal field. The experimental results are given in Fig. 8. The resonance intensity maximum was obtained at $\theta = 50°$, the minimum at 0° and 90°. In the authors' opinion this result is in accordance with the theory of Ref. 18. However, it is worth noticing that this theory had been developed for the wave propagation direction along the [100] axis, but not for [110]. L-MAR at higher frequencies (600–1000 MHz) was investigated in Refs. 57, 58. Though the authors of Ref. 56 used samples of the same orientation and shape as in Ref. 56, the magnetoelastic coupling efficiency maximum was found at $\theta = 90°$.

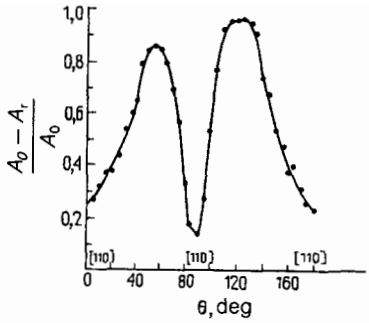

FIG. 8. MAR anisotropy of a YIG sample in the (100) plane at $f = 221$ MHz. A_r, A_0—sound pulse amplitude at resonance and far from it (at higher fields) respectively.[56]

L-MAR in conditions of the uniformity of the internal field was the subject of Refs. 10, 22. For this purpose either spherical samples with small plane areas for attaching transducers or cylindrical samples placed inside polycristalline YIG spherical shells were used. Apart from the ordinary methods of MAR investigation by external field scanning, the resonance was studied in Ref. 22 at several values of hypersound region frequencies. In this experiment resonance absorption had not been found for [100] and [111] oriented samples if the L-wave propagated in a parallel or orthogonal direction to that of the magnetic field. Resonance absorption peaks were observed at all other values of θ. In the [110] sample at $\theta = 90°$ the magnetoelastic coupling exists at some angles between the field direction and

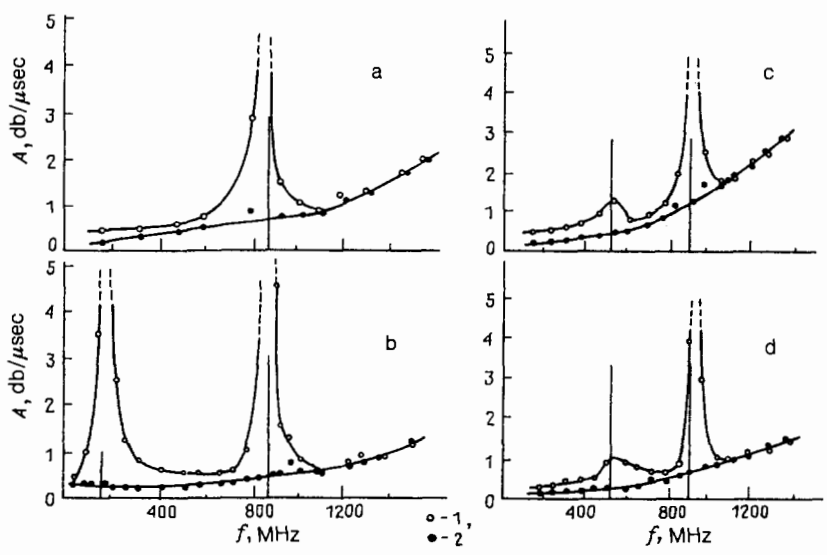

FIG. 7. Frequency dependence of longitudinal (a,c) and shear (b,d) elastic waves propagating in a YIG single crystal along [111] (a,b) and [110] (c,d). Vertical lines are calculated positions and relative intensity of absorption lines. *1*—$H_0 = 0$, *2*—$H_0 = 4000$ Oe.[54]

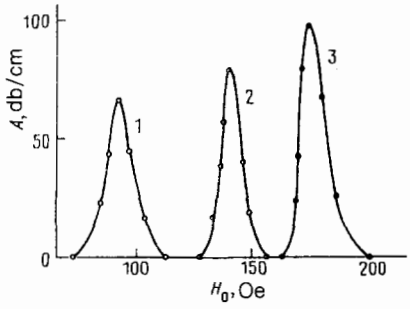

FIG. 9. Resonance absorption lines of longitudinal elastic waves at 1110 (*1*), 1290 (*2*) and 1470 MHz (*3*). Waves propagate in a YIG crystal along the [110] axis perpendicularly to H_0. Angle between the field direction and the [001] axis is $\beta = 45°$ (Ref. 22).

the crystallographic directions (Fig. 9). It should be noted that due to the influence of relativistic internal fields the effective gyromagnetic ratio[22] exceeded the same for the free electron spin (2.8 MHz/Oe) and changed from 11 to 8 MHz/Oe at the higher frequency. The angular dependence of S-MAR depth (Fig. 10) was in agreement with the theoretical prediction of the possibility of observing the resonance in transverse magnetic fields when $\mathbf{k}\|\mathbf{H}_0$.

HF L-MAR (1000 MHz) in a YIG spherical single crystal in a transverse magnetic field was observed in Ref. 59. Several absorption peaks were observed at different values of the external magnetic field. It means that there are several MAR branches caused by the presence of domain structure.

Nonlinear interaction of two shear waves propagating along the [111] axis of a YIG single crystal towards each other was investigated in Ref. 60. The cylindrical sample was placed between the central electrodes of two coaxial resonators so that most of its volume was inside the HF resonator capacitance gap. An external uniform magnetic field was applied transversely to the sample axis. An electromagnetic signal of double the frequency corresponding to the moment of meeting of the elastic pulses was recorded. It follows from the experiment that at a particular value of the external field the interaction is located in a small region of the crystal (estimated to be less than 2 mm). When the magnetic field increases the interaction region shifts towards the sample center due to the internal field distribution features under the experimental conditions. The interaction of these elastic waves may lead under some conditions to a nonlinear effect of excitation of magnetization oscillations of double the frequency with $\mathbf{k} = 0$. The resulting signal represents a convolution of the initial signals.

The results of the investigation of L-wave second harmonic generation are presented in Ref. 30. The 560 MHz frequency longitudinal wave propagated along the main crystallographic directions in a single crystal YIG sphere. The generation of the second harmonic was observed for all these directions. An analysis of all probable sources of nonlinearity (surface and volume ones) is presented. The conclusion is drawn concerning the volume character of the crystal nonlinearity. Two peaks of the second harmonic absorption were observed at resonance field values for single and double frequency values (Fig. 11). The observed doublet is in rather good agreement with that calculated by Eq. (1.29). It was impossible to observe an increase of the second harmonic amplitude at resonance under the experimental conditions. The second harmonic pulses completely disappeared due to the extremely strong increase of elastic wave absorption.

Almost all the discussed results were obtained at rather high frequencies and, consequently, in high magnetic fields. These fields significantly alter the initial domain structure of the sample. In this connection Refs. 23, 26, 31–34, 53, 61–67, carried out at frequencies near 30 MHz are of definite interest. As noted above, LF MAR makes it possible to get information about the dynamics of the internal field in the course of the sample magnetization process. This makes possible studies of the real structure of magnetic materials.

In these experiments linear and nonlinear magnetoacoustic spectra were obtained. The linear magnetoacoustic spectrum is the dependence on H_0 of the amplitude A_ω of the first pulse transmitted through the sample at the excitation frequency, and the nonlinear one is the same at the higher harmonic frequency: $A_{2\omega}$ or $A_{3\omega}$ etc. The samples used in the experiments were made of YIG and Mn-Zn spinel (MZS)

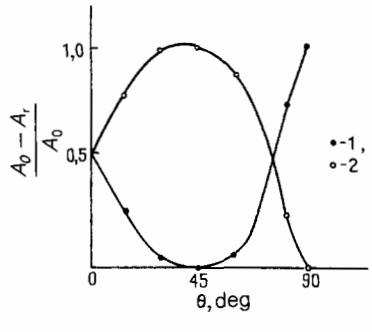

FIG. 10. Angular dependence of MAR for propagation of shear waves ($f = 1100$ MHz) along [100] in a YIG single crystal. *1*—elastic waves are polarized in the plane containing $\mathbf{k}$ and $\mathbf{H}_0$, *2*—they are polarized orthogonally to this plane.[22]

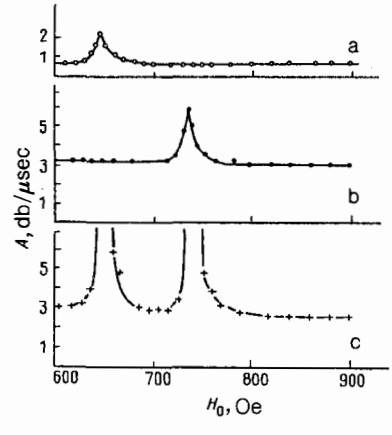

FIG. 11. Dependence of the longitudinal elastic waves damping on $\mathbf{H}_0$ for propagation along the [100] axis. a—linear MAR at 560 MHz, b—linear MAR at 1120 MHz, c—560 MHz elastic waves are propagating and the second harmonic at 1120 MHz is observed.[30]

single crystals. Most of them had an intrinsic FMR line width smaller than the effective field $H_{eff} \sim 11$ Oe. In this case the condition of Eq. (2.14) for resonance to be observed was satisfied.

The publications 31, 32, 61, 62, 64, 65 are dedicated to comparative investigations of linear and nonlinear S-MAR. In contrast to the linear MAR, the nonlinear MAR had been observed very clearly in all the investigated crystals (see Table II). The nonlinear S-MAR profile has a well-defined canonical form (Fig. 12).

We shall analyze the linear S-MAR spectra in detail. Figure 13 presents S-spectra $A_\omega(H_0)$ for YIG at two frequencies: 6.82 MHz (1) and 30 MHz (2). Notice must be taken of a small resonance profile dependence on the frequency. An important feature of the LF MAR is that the derivative $\partial f_r/\partial H_0$ is large ($\gamma^* \approx 6$ MHz/Oe) and, hence, such a small frequency change is not expected to shift the profile to any considerable extent. The resolution of the analysis grows as the frequency increases: fine structure can be seen very distinctly in spectrum 2.

The asymmetry of the crystal domain structure with respect to its center causes a noticeable change of MAR spectra if the external field direction is reversed (see Fig. 14). It must be noted that if the sample is rotated with respect to the external magnetic field direction then, besides the change in the magnetoelastic coupling efficiency, a change of the demagnetizing tensor components will occur. This results in the resonance shift into the region of higher fields. The resonance becomes less pronounced and disappears at $\theta = 90°$.

We shall now discuss the conditions for the experimental observation of MAR phenomena associated with longitudinal and shear waves. Turning back to Fig. 3 we can see that the effective field $\mathbf{H}_{eff}$ can have any direction inside the sphere of f/γ radius (see Eq. (2.1)). It follows from the Bloch–Landau equation (1.3) that the forced spin precession occurs around the direction of the effective field $\mathbf{H}_{eff}$ and is possible if $\mathbf{H}_{eff}$ and the vector of the alternating magnetostriction field $\mathbf{h}$ produced by the elastic wave are not collinear. This is the reason why S-MAR can not be observed in an ideal single-domain crystal if the sound wave propagates along the main crystallographic directions and the external field direction is orthogonal to $\mathbf{k}$, and L-MAR can not be observed if $\mathbf{H}_0 \| \mathbf{k}$. The fact that the authors of Refs. 22, 38, and 42 observed S-MAR when $\mathbf{H}_0 \perp \mathbf{k}$ can be explained by imperfect magnetic ordering and by the features of the domain structure of the examined samples.

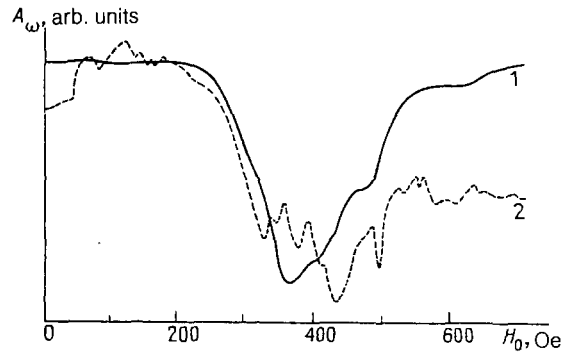

FIG. 13. Linear magnetoacoustic S-spectra of YIG: *1*—6.82 MHz, *2*—30 MHz.

The observation of linear L-MAR was impossible in MZS crystals with developed domain structure.[26,53] At fields within the range of 1.2–1.4 kOe, the domain structure was intensively rearranged accompanied by a quite rapid sound attenuation decrease. In Bridgman crystals of MZS the linear L-MAR could not be observed against the background of these processes in any of the studied crystallographic directions. L-MAR was observed only in the Verneuil-grown MZS crystal of the [110] orientation (Fig. 15). The sample had a lower iron content and, probably, had a small number of domains.

Nonlinear LF S-MAR was studied using second harmonic magnetoacoustic spectra $A_{2\omega}(H_0)$.[61,62,64,65] For a longitudinal direction of the external field the nonlinear S-MAR was observed in almost all the studied crystals. The exceptions were MZS crystals with high initial attenuation (for example, unannealed ones). The nonlinear magnetoacoustic spectra have a pronounced fine structure. Note that

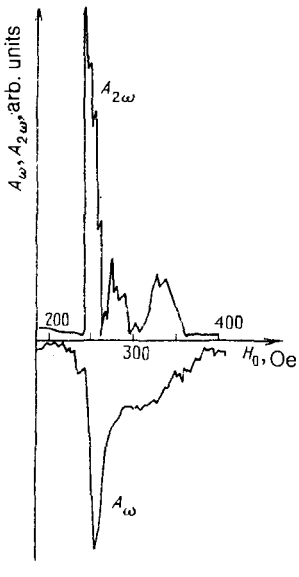

FIG. 12. Linear $A_\omega(H_0)$ and nonlinear $A_{2\omega}(H_0)$ S-MAR in Verneuil-grown MZS (the [110] orientation).[32]

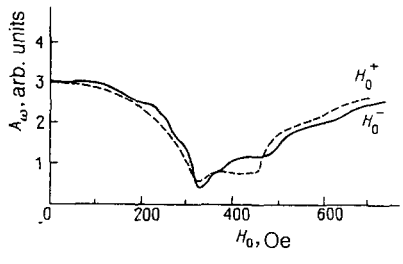

FIG. 14. Linear magnetoacoustic S-spectrum of a YIG crystal for opposite directions of the external magnetic field.[31]

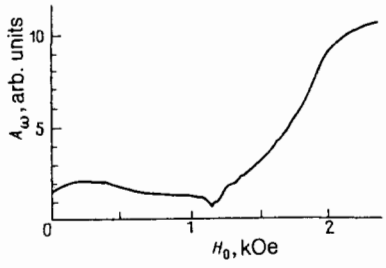

FIG. 15. Linear L-MAR in Verneuil-grown MZS (the [110] orientation).[26]

in the nonlinear spectrum $A_{2\omega}(H_0)$ the field resolution increases by $\sqrt{2}$ times in case of the Gaussian shape of the intrinsic FMR line. The oscillations of $A_{2\omega}(H_0)$ profile in MAR region are caused by the internal field inhomogeneity and, probably, by high velocity dispersion. Figure 16 illustrates the greater clarity of the nonlinear S-MAR in comparison with the linear one.

We shall now discuss the possibilities of the internal magnetic field control. It follows from the above discussion that the S-MAR profile width ΔH is determined by the difference of the internal field values in the center and at the ends of the crystal. In order to diminish ΔH, the field should be made more uniform. In the limit of elliptical samples with a uniform field in the absence of magnetically charged defects, the profile width is equal to ΔH_i for a specified frequency and the corresponding internal field value. The internal field can be controlled by a relatively weak inhomogeneous constant magnetic bias field $\mathbf{h}_0$. In order to do this a coil of 40 turns of copper wire about 3 mm in linear dimension was wound around the middle part of the MZS crystal in Ref. 63. The coil was connected to a dc power unit. Figure 17 demonstrates the S-spectra $A_{2\omega}(H_0)$ at 28.5 MHz frequency: (a)—without bias field, (b), (c)—the bias field has a value of + 12 Oe and -12 Oe with respect to the external field $\mathbf{H}_0$. It is evident from Fig. 17 that with a positive $\mathbf{h}_0$ the resonance is shifted towards smaller external fields (the

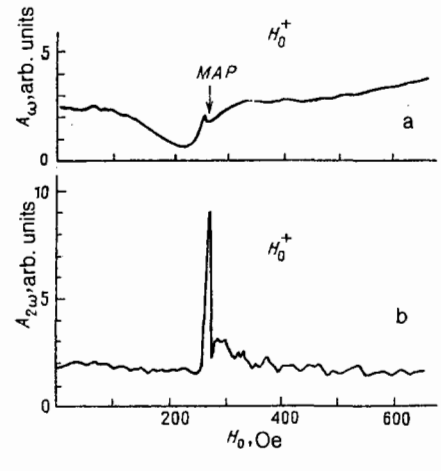

FIG. 16. Linear (a) and nonlinear (b) S-spectra of annealed MZS (the [100] orientation).[32]

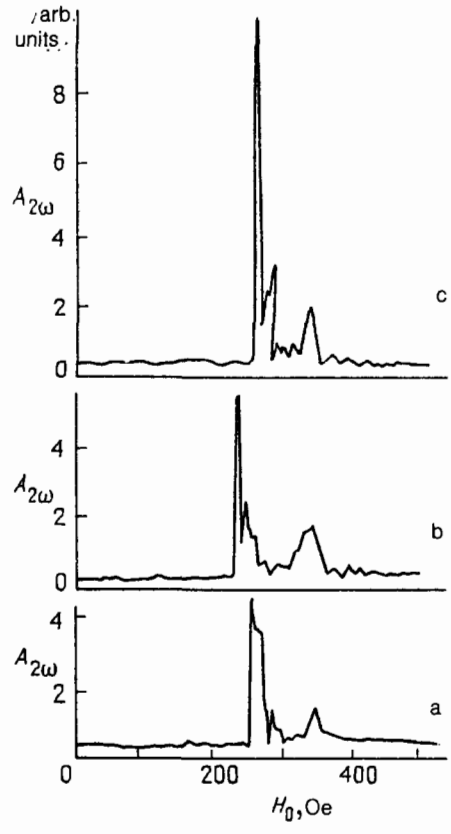

FIG. 17. Effect of a weak constant nonuniform bias field $\mathbf{h}_0$ on the S-MAR profile in a Verneuil MZS crystal (the [110] orientation).[63]

inhomogeneous field adds to H_0) and the profile is slightly narrowed. Conversely, a negative $\mathbf{h}_0$ shifts the resonance towards higher external fields and due to "smoothening" of the internal field leads to a significant narrowing of the main peak and the total resonance width ΔH. The resonance amplitude increases by a factor of 4. The minimum width of the onset peak in Ref. 63 is about 2 Oe. It means that the intrinsic FMR line width of such a MZS crystal is smaller than 2 Oe.

It was shown in Sec. 1 that in the resonance region the effectiveness of the magnetoelastic coupling increases abruptly. Hence, the sound absorption increases[30] as well as the efficiency of the higher harmonic generation due to the extremely high nonlinearity of the spin system. Competition between these processes does not always lead to the prevalence of the absorption. The S-spectra $A_{2\omega}(H_0)$ of a YIG crystal[32,61] indicate that in near-resonance fields the signal is almost completely transformed into a weak signal of double the frequency. As was already mentioned, in the case of an inhomogeneous internal field, the resonance is localized in a definite region δz. If the external magnetic field varies in the resonance range this region moves over the crystal volume. In other words, under these conditions the crystal becomes an extremely inhomogeneous nonlinear medium: in regions of size $\sim\delta z$ higher harmonic generation occurs and dissipation due to the nonlinear absorption occur. In other nonresonant regions these processes are determined by the slightly renormalized higher-order elastic constants and by relaxation. The YIG lattice nonlinear elastic constants are quite

small and the nonlinear parameter value outside resonance is $\Gamma_0 \simeq 2$. The ratio of the effective nonlinear parameter Γ calculated using the $A_{2\omega}(H_0)$ measurements (on the assumption of harmonic generation over the entire length) to Γ_0 is plotted as a function of H_0 in Fig. 18. Estimates[32,61] show that with a resonance the profile width $\Delta H \approx 170$–200 Oe, with resonance absorption $\alpha^s_{p_r} = 21.4\ \mathrm{cm}^{-1}$ and $\Delta H_i \approx 1$ Oe the resonance region at the center of the crystal according to Eq. (2.9) has a size $\delta z \approx 5 \cdot 10^{-2}$ cm, and $2\alpha_p \delta z = 2.14$. Hence, inequalities (2.12) and (2.13) are not fulfilled. The spectra $A_\omega(H_0)$ and $A_{2\omega}(H_0)$ have dissipative distortions in the region of onset of resonance as illustrated by Fig. 19 (the second curve). The closer to the crystal ends, the smaller is the size of the resonance region and the less pronounced the dissipative distortions of the spectra. At the ends of the crystal the relation (2.8) yields $2\alpha_p \delta z \approx 0.08$. In the region of resonant termination the mean value of Γ/Γ_0 is about $4 \cdot 10^2$. According to (2.8), here we have $L/2\delta z = 2(\Delta H/\Delta H_i) \approx 400$ and, therefore, the resonance value of Γ_r/Γ_0 is at least 10^5. A more accurate evaluation of Γ_r/Γ_0 is difficult because the leading and, especially, the trailing edges of the MAR profile are not quite distinct, while the value of δz is tentative.

In MZS crystals, the dissipative distortions of the S-MAR profile were less pronounced even at the beginning of the resonance. For the Verneuil-grown crystal of [110] orientation the ratio Γ_r/Γ_0 was estimated to be 400 ± 100 (at the center of the crystal).

A thorough investigation of nonlinear magnetoacoustic resonance on longitudinal waves was carried out in Refs. 26, 53. The L-MAR profile for thin long (in the direction of **k**) samples must differ from the canonical profile of S-MAR (Fig. 4). In the case of L-MAR the resonance regions are fundamentally three-dimensional ones because of the transverse direction of the external field. The experimental profile of $A_{2\omega}(H_0)$ is illustrated by the second curve in Fig. 20. It is remarkable that the smooth onset of the nonlinear L-MAR occurs (especially for [100] crystals) well before the growth of $A_\omega(H_0)$ (the first curve). The profile of the nonlinear S-MAR in a longitudinal field in crystals of [100] orientation has an abrupt leading edge (see above). This can be explained by the predominance of 180° domain structure and a small initial quantity of 90° domains in crystals of this form. Under the L-MAR conditions, the increasing transverse

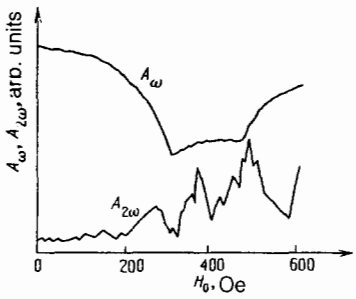

FIG. 19. Linear $A_\omega(H_0)$ and nonlinear $A_{2\omega}(H_0)$ S-spectra in a YIG crystal ($\mathbf{H}_0 \| \mathbf{k} \| [100]$).[32]

field forms a 90° domain structure. The resonance in such domains occurs in lower fields than required for the resonance at the core of the crystal, where a maximum of $A_{2\omega}$ is subsequentially attained. This explains the smooth leading edge of the profile. It must be noted that the resonance onset field and the maximum $A_{2\omega}$ field depend upon the orientation of the crystal and the geometry of experiment.

The second harmonic generation is caused by the quadratic nonlinearity of the magnetoelastic coupling. However under MAR conditions higher harmonic generation is also possible. Third harmonic generation was observed in Ref. 66. The magnetoacoustic spectra $A_{3\omega}$ and $A_{2\omega}$ of a YIG sample are shown in Fig. 21. These spectra correspond to different phonon-magnon coupling processes (for three- and four-particle interactions, respectively). A possibility of the third harmonic generation arises in weak external fields (~ 200 Oe). The second harmonic amplitude under these conditions is small, hence a probability of a quadratic process $2\omega + \omega = 3\omega$ is also small. A more probable mechanism for the $A_{3\omega}$ generation is the cubic nonlinearity of the Bloch–Landau equation (1.3), caused by the anisotropy field. It is known that the competition between the anisotropy and the exchange fields leads to creation of a domain boundary. Thus the forming of a weak-field maximum of $A_{3\omega}(H_0)$ spectrum most probably is caused by the cubic nonlinearity of domain boundaries. At higher fields a third-harmonic generation process as a result of the nonlinear interaction of the first and the second harmonics on the quadratic nonlinearity predominates. Their difference is also determined by the competition of local generation and dissipation processes.

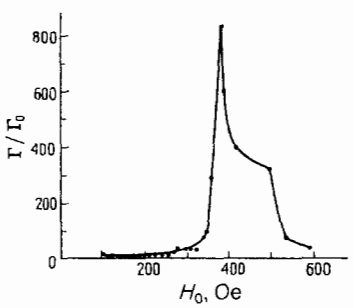

FIG. 18. Dependence of the ratio of the effective nonlinear parameter Γ to its non-resonant value Γ_0 on H_0 for a shear wave in a YIG crystal.[61]

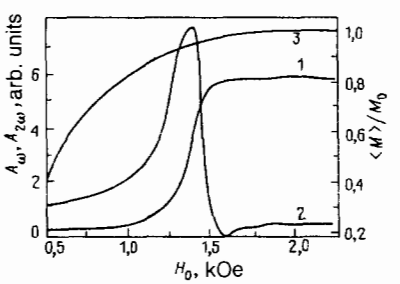

FIG. 20. Magnetoacoustic spectra (*1*—$A_\omega(H_0)$, *2*—$A_{2\omega}(H_0)$) and normalized average magnetization—*3* in Bridgman-grown MZS (the [100] orientation).[53]

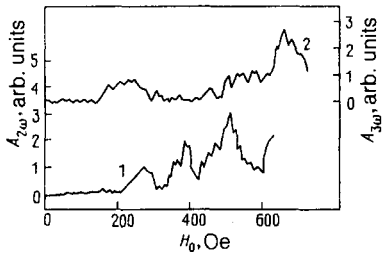

FIG. 21. Nonlinear magnetoacoustic spectra $A_{2\omega}(H_0)$ and $A_{3\omega}(H_0)$ of a YIG crystal.[66] The gain of the receiving channel for the third harmonic is by a factor of 10 greater than for the second harmonic.

4. INTERNAL MAGNETIC FIELD RECONSTRUCTION USING THE MAR PROFILE

In a thin long crystal the S-MAR profile not subjected to strong dissipative distortions can be used to reconstruct the internal field structure that changes in the process of magnetization.[32] The field is assumed to be symmetric with respect to the center ($z = 0$) of the crystal. Relations (2.6), (2.10) and (2.11) imply the proportionality of $A_\omega(H_0)$ and $A_{2\omega}(H_0)$ to dz/dH_{in} if condition (2.12) is satisfied. As a result, integration of the MAR profile over H_0 yields the $z(H_{in})$ function. The inverse z^{-1} function represents the internal field distribution $H_{in}(z)$. The latter for a Verneuil-grown MZS crystal cut along the [110] axis is demonstrated in Fig. 22. The MAR profile used for this reconstruction is shown in Fig. 12. We must note that the field at the center of the crystal is reconstructed at the moment when the crystal is not yet magnetically saturated. Meanwhile, reconstruction at the crystal ends is made when the bulk of the crystal is already magnetized to saturation. The internal field is not quite smooth. This is probably due to the domain structure and (or) the defects of the crystal. Such extended structures can be seen in the one-dimensional tomogram of the crystal. As for small magnetically charged defects, they are masked (see Sec. 2) and do not show up in the MAR spectrum. Under the above conditions the internal field can be reconstructed even in the case of a complex configuration of magnetics, where theoretical calculations of the field are very complicated.

Such a reconstruction method using linear or nonlinear MAR profile has advantages over the method[68,69] using the delay time of the received acoustic pulse with respect to the initiating electromagnetic pulse. Internal field investigation in principle becomes possible in electrically conducting magnetically ordered crystals because of the nonelectromagnetic method of exciting the magnetoelastic wave. The skin-layer limitations are therefore avoided. The efficiency of the excitation and reception of magnetoelastic waves increases as well as the signal-to-noise ratio (the surrounding electromagnetic field greatly affects the small useful signal in the method of Refs. 68, 69).

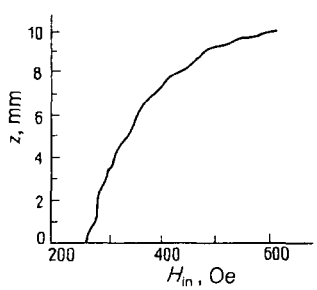

FIG. 22. Internal field $H_{in}(z)$ in a Verneuil crystal of MZS reconstructed from the $A_{2\omega}(H_0)$ profile presented in Fig. 12.[32]

Let us discuss in detail some features of HF and LF MAR application to nondestructive testing. The former operates at frequencies of the order of 10^{10} Hz when the external fields needed to achieve the resonance condition are rather high (several kOe). Under these conditions the crystal usually is magnetized to saturation and becomes a single-domain one. LF MAR operates at frequencies of the order of $10^6 - 10^7$ Hz, when H_0 is insufficient for a drastic change in the original distribution of the internal field. Usage of high or low frequencies depends upon the aims of flaw detection. If the only task is to trace crystal defects such as dislocations, microcracks and so on then HF MAR is more suitable because the domain structure practically has no effect on the measurements. LF MAR is preferable if one has to know not only the defects of the structure but also the real initial internal field distribution including the domain structure. The second reason for using low frequencies is that the sound wave attenuation depends quadratically on frequency, so in poor-quality crystals the attenuation at high frequencies can be too high for performing precise measurements.

CONCLUSION

Summarizing, we must note that MAR as a resonance interaction of elastic and spin waves was observed in single crystals with sufficiently high magnetic order. The necessary condition for MAR observation is that the intrinsic FMR line width must be smaller than the effective resonance field value. This implies the condition of $f\tau > 1$, where τ is the spin-spin relaxation time. In inhomogeneous internal magnetic fields MAR occurs in the regions where the direction of the magnetic moment coincides with that of the external magnetic field. The competition of the resonance absorption and the giant quadratic nonlinearity may lead to an abrupt increase of the second acoustic harmonic amplitude. This effect is known as nonlinear MAR. Under these conditions the crystal becomes an extremely nonlinear-inhomogeneous medium. The giant nonlinearity region can be shifted along the crystal by the external magnetic field. The nonlinear MAR application increases the resolution of MAR-spectroscopy and allows a more detailed study of the magnetic subsystem nonlinearity.

There are certain difficulties in experimental identification of magnetoacoustic resonance in real magnetic materials. As a rule MAR occurs against the background of other nonresonant processes. In the presence of micro- and macroinhomogeneities of crystal structure and those of the internal field there is a possibility of other relaxation magnetic absorption processes, besides the "pure acoustical" ones (scattering, lattice absorption). They depend, naturally, on the external magnetic field. There is still some doubt whether some observations reported in early publications on

this subject that were reviewed above actually refer to MAR. Certain confirmation can be made by additional investigations of the polarization plane rotation in acoustic waves and of the velocity dispersion. The simultaneous observation of the linear and the nonlinear MAR significantly increases the reliability of MAR observations because the possible interfering processes have a comparatively weak nonlinearity. The HF MAR nonlinear spectra at comparatively high frequencies should exhibit a doublet structure.

MAR spectroscopy of inhomogeneous magnetic materials in single-domain approximation allows one to reconstruct the internal fields during the magnetization process. Nevertheless magnetically charged defects can be observed better by MAR-spectra because the latter represent a differential picture of the internal field. The investigation of fine structure of MAR-spectra is a key for new methods of ferrite diagnostics. These materials have a wide application in modern electronic and computer technology. The use of the giant nonlinearity of the crystalline ferrodielectrics offers exceptional opportunities in radio signal processing devices. The parameters of the latter can be controlled by an external magnetic field within wide limits.

[1)] Sometimes parametric excitation of acoustic oscillations by an electromagnetic wave[6] is referred to in the literature as "magnetoacoustic resonance."

[2)] We note here that the theory of magnetoelastic coupling[2] that takes into account the rotational invariance of the initial equations can for such "strong" effects as MAR, be substituted for by the approximate theory[11] used in the present paper.

[1] E. A. Turov and V. G. Shavrov, Usp. Fiz. Nauk **140**(3), 429 (1983) [Sov. Phys. Usp. **26**, 593 (1983)].
[2] V. G. Bar'yakhtar and E. A. Turov, Magnetoelastic Excitations, in *Spin Waves and Magnetic Excitations 2*, (Eds.) A. S. Borovik-Romanov and S. K. Sinha, Elsevier Science Publ. B. V., 1988, p. 333.
[3] A. I. Akhiezer, V. G. Bar'yakhtar, and S. V. Peletminskiĭ, Zh. Eksp. Teor. Fiz. **35**, 228 (1958) [Sov. Phys. JETP **8**, 157 (1959)].
[4] C. Kittel, Phys. Rev., **110**, 836 (1958).
[5] S. V. Peletminskiĭ, Zh. Eksp. Teor. Fiz. **37**, 452 (1959) [Sov. Phys. JETP **10**, 321 (1960)].
[6] Ya. A. Monosov, *Nonlinear Ferromagnetic Resonance* (In Russian), Nauka, M., 1971.
[7] R. C. Le Crow and R. Comstock, in *Physical Acoustics: Principles and Methods* (Ed.) W. P. Mason, v. 3B, Academic, N. Y., London, 1966 [Russ. transl., Mir, M., 1968, p. 156].
[8] W. Strauss in *Physical Acoustics: Principles and Methods* (ed. by W. P. Mason), v. 4B, Academic, N. Y., 1968, [Russ. transl., Mir, M., 1970, p. 247].
[9] I. W. Tucker and V. W. Rampton, *Microwave Ultrasonics in Solid State Physics*, North-Holland, Amsterdam, 1972. [Russ. transl., Mir, M., 1975].
[10] V. V. Lemanov and G. A. Smolenskiĭ, Usp. Fiz. Nauk **108**, 465 (1972) [Sov. Phys. Usp. **15**, 708 (1973)].
[11] V. V. Lemanov in *Physics of Magnetic Dielectrics*, (Ed.) G. A. Smolenskiĭ, (In Russian) Nauka, 1974, p. 284 L.
[12] A. I. Akhiezer, V. G. Bar'yakhtar, and S. V. Peletminskiĭ, *Spin Waves*, North-Holland, Amsterdam Wiley, N. Y., 1968. [Russ. original, Nauka, M., 1967].
[13] V. I. Ozhogin and B. L. Preobrazhenskiĭ, Usp. Fiz. Nauk **155**, 593 (1988) [Sov. Phys. Usp. **31**, 713 (1988)].
[14] V. A. Shutilov, N. V. Charnaya, and L. N. Kotov, Pis'ma Zh. Tekh. Fiz. **12**, 1060 (1986) [Sov. Tech. Phys. Lett. **12**, 438 (1986)].
[15] M. V. Manuilov, V. S. Bondarenko, and V. V. Krinochkin, Pis'ma Zh. Tekh. Fiz. **12**, 599 (1986) [Sov. Tech. Phys. Lett. **12**, 246 (1986)].
[16] B. Luthi, Phys. Konden. Mater. **1**, 197 (1963).
[17] G. A. Smolenskiĭ and V. V. Lemanov, *Ferrites and Their Technical Applications*, (In Russian), Nauka, L., 1975.
[18] B. Kh. Ishmukhametov, Fiz. Met. Metalloved. **17**, 323 (1964) [Phys. Met. Metallogr. (USSR) **17**(3), 1 and **17**(5), 1 (1964)].
[19] K. B. Vlasov and B. Kh. Ishmukhametov, Zh. Eksp. Teor. Fiz. **36**, 130 (1959) [Sov. Phys. JETP **9**, 921 (1959)].
[20] E. Schlomann, J. Appl. Phys. **31**, 1647 1960.
[21] H. Matthews and R. C. Le Craw, Phys. Rev. Lett. **8**, 397 1962.
[22] V. V. Lemanov, A. V. Pavlenko, and A. N. Grishmanovskiĭ, Zh. Eksp. Teor. Fiz. **59**, 712 (1970) [Sov. Phys. JETP **32**, 389 (1970)].
[23] L. K. Zarembo and S. N. Karpachev, Akust. Zh. **32**, 832 (1986) [Sov. Phys. Acoust. **32**, 519 (1986)].
[24] B. A. Auld in: *Applied Solid State Science* (Ed.) R. Wolfe, NY–London, Academic, 1971, v. 2, p. 2.
[25] E. H. Turner, Phys. Rev. Lett., **5**, 100 (1960).
[26] O. Yu. Belyaeva, L. K. Zarembo, and S. N. Karpachev, Fiz. Tverd. Tela (Leningrad) **30**, 1873 (1988) [Sov. Phys. Solid State **30**, 1081 (1988)].
[27] A. L. Polyakova, Akust. Zh. **22**, 427 (1976) [Sov. Phys. Acoust. **22**, 238 (1976)].
[28] D. I. Anikeev, L. K. Zarembo, S. N. Karpachev *et al.*, Fiz. Met. Metalloved. **55**, 622 (1983) [Phys. Met. Metallogr. (USSR) **55**, 192 (1983)].
[29] L. K. Zarembo, S. N. Karpachev, and V. V. Sukhovtsev, Pis'ma Zh. Tekh. Fiz. **7**, 1082 (1981) [Sov. Tech. Phys. Lett. **7**, 464 (1981)].
[30] A. N. Grishmanovskiy, N. K. Yushin, V. L. Bogdanov, and V. V. Lemanov, Fiz. Tverd. Tela (Leningrad) **13**, 1833 (1971) [Sov. Phys. Solid State **13**, 1537 (1971)].
[31] L. K. Zarembo and S. N. Karpachev, Fiz. Tverd. Tela (Leningrad) **26**, 1943 (1984) [Sov. Phys. Solid State **26**, 1178 (1984)].
[32] L. K. Zarembo and S. N. Karpachev, Zh. Eksp. Teor. Fiz. **93**, 1499 (1987) [Sov. Phys. JETP **66**, 855 (1987)].
[33] L. K. Zarembo and S. N. Karpachev in *Problems of Nonlinear Acoustodiagnostics* (in Russian) (Ed.) N. D. Veksler, Valgus, Tallinn, 1986, p. 125.
[34] L. K. Zarembo and S. N. Karpachev, Akust. Zh. **35**, 51 (1989) [Sov. Phys. Acoust. **35**, 30 (1989)].
[35] E. G. Spencer and R. C. Le Craw, Phys. Rev. Lett. **1**, 241 (1958).
[36] H. Bommel and K. Dransfeld, Phys. Rev. Lett. **3**, 83 (1959).
[37] H. Bommel and K. Dransfeld, Bull. Am. Phys. Soc. (ser. 2) **5**, 58 (1960).
[38] B. Luthi, Phys. Lett. **3**, 285 (1963).
[39] B. Luthi and F. Oertle, Phys. Kondens. Mater. **2**, 99 (1964).
[40] B. Luthi, Helv. Phys. Acta, **37**, 185 (1964).
[41] B. Luthi, Appl. Phys. Lett., **6**, 234 (1965).
[42] B. Luthi, J. Appl. Phys., **37**, 990 (1966).
[43] B. Luthi and T. Henningsen in *Proc. of Intern. Conf. Magnetism*, Nottingham, 1964, London, 1965, p. 668.
[44] B. Luthi, Appl. Phys. Lett., **8**, 107 (1966).
[45] B. Luthi, Solid State Commun. **5**, 319 (1967).
[46] E. G. Spencer, R. T. Denton, and R. P. Chambers, Phys. Rev. **125**, 1950 (1962).
[47] G. A. Smolenskiĭ and A. Nasyrov, Izv. Akad. Nauk SSSR, Ser. Fiz., **30**, 998 (1966) [Bull. Acad. Sci. USSR Phys. Ser. **30**(6), 1041 (1966)].
[48] A. Nasyrov and A. V. Pavlenko, Fiz. Tverd. Tela (Leningrad) **9**, 276 (1967) [Sov. Phys. Solid State **9**, 205 (1967)].
[49] A. N. Grishmanovskiĭ, Fiz. Tverd. Tela (Leningrad) **16**, 2716 (1974) [Sov. Phys. Solid State **16**, 1755 (1975)].
[50] A. V. Pavlenko, Yu. M. Yakovlev, and V. V. Lemanov, Fiz. Tverd. Tela (Leningrad) **11**, 3300 (1969) [Sov. Phys. Solid State **11**, 2673 (1970)].
[51] A. N. Grishmanovskiĭ, V. V. Lemanov, and G. A. Smolenskiĭ, Fiz. Tverd. Tela (Leningrad), **14**, 2369 (1972) [Sov. Phys. Solid State **14**, 2050 (1973)].
[52] H. Matthews and E. R. Morgenthaler, Phys. Rev. Lett. **13**, 614 (1964).
[53] L. K. Zarembo, S. N. Karpachev, Dokl. Akad. Nauk SSSR **289**, 1362 (1986) [Sov. Phys. Dokl. **31**, 658 (1986)].
[54] V. V. Lemanov and A. V. Pavlenko, Zh. Eksp. Teor. Fiz. **57**, 1528 (1969) [Sov. Phys. JETP **30**, 826 (1970)].
[55] V. V. Lemanov, A. V. Pavlenko, and O. V. Shakin, Pis'ma Zh. Eksp. Teor. Fiz. **8**, 242 (1968) [JETP Lett. **8**, 148 (1968)].
[56] G. A. Smolenskiĭ and A. Nasyrov, Fiz. Tverd. Tela (Leningrad) **7**, 3704 (1965) [Sov. Phys. Solid State **7**, 3002 (1966)].
[57] K. V. Goncharov, V. A. Krasilnikov, and V. I. Uchastkin, Fiz. Tverd. Tela (Leningrad) **9**, 3384 (1967) [Sov. Phys. Solid State **9**, 2671 (1968)].
[58] M. F. Lewis and D. G. Scotter, Phys. Lett. **28A**, 303 (1968).
[59] G. F. Gusyatskiĭ, A. A. Vetrov, and E. M. Smokotin in *Magnetic and Resonance Properties of Magnetic Materials* (Ed.) by G. A. Petrakovskiy (in Russian), SO AN SSSR, Krasnoyarsk, 1980, p. 171.
[60] N. K. Yushin, A. N. Grishmanovskiĭ, and V. V. Lemanov, Fiz. Tverd. Tela (Leningrad) **16**, 1569 (1974) [Sov. Phys. Solid State **16**, 1025 (1975)].
[61] L. K. Zarembo, S. N. Karpachev, and S. Sh. Gendelev, Pis'ma Zh. Tekh. Fiz. **9**, 502 (1983) [Sov. Tech. Phys. Lett. **9**, 217 (1983)].
[62] L. K. Zarembo and S. N. Karpachev, Fiz. Tverd. Tela (Leningrad), **25**, 2343 (1983) [Sov. Phys. Solid State **25**, 1345 (1983)].
[63] L. K. Zarembo, S. N. Karpachev, and S. Sh. Gendelev, Pis'ma Zh. Tekh. Fiz. **10**, 1050 (1984) [Sov. Tech. Phys. Lett. **10**, 447 (1984)].
[64] S. G. Abarenkova, S. Sh. Gendelev, and L. K. Zarembo, Fiz. Tverd.

Tela (Leningrad) **27**, 2450 (1985) [Sov. Phys. Solid State **27**, 1467 (1985)].
[65] L. K. Zarembo and S. N. Karpachev, Fiz. Tverd. Tela (Leningrad) **28**, 311 (1986) [Sov. Phys. Solid State **28**, 173 (1986)].
[66] O. Yu. Belyaeva, L. K. Zarembo, and S. N. Karpachev, Vestn. Mosk. Univ. Fiz. Astron., **28**, 50 (1987).
[67] L. K. Zarembo and S. N. Karpachev, Defektoskopiya No. 1, p. 21 (1987) [Sov. J. Nondestr. Test. (1987)].
[68] J. R. Eshbach, Phys. Rev. Lett. **8**, 357 (1962).
[69] J. R. Eshbach, J. Appl. Phys. **34**, 1298 (1963).

English text supplied by the authors